Check for updates

Journal of Sensor Science and Technology
Vol. 30, No. 4 (2021) pp. 210-217
http://dx.doi.org/10.46670/JSST.2021.30.4.210
pISSN 1225-5475/eISSN 2093-7563

α-Fe_2O_3 nanostructure-based gas sensors

Seonyong Lee[1] and Ho Won Jang[1,2,+]

Abstract

Gas sensors based on semiconducting metal oxides have attracted considerable attention for various applications owing to their facile, cheap, and small-scale manufacturing processes. Hematite (α-Fe_2O_3) is widely considered as a promising candidate for a gas-sensing material owing to not only its abundance in the earth's crust and low price but also its chemical stability and suitable bandgap energy. However, only a few studies have been performed in this direction because of the low gas response and sluggish response of hematite-based gas sensors. Nanostructures present a representative solution to both overcome these disadvantages and exploit the desirable features to produce high-performance gas sensors. However, several challenges remain for adopting gas sensors based on metal oxide nanostructures, such as improving cost efficiency and facilitating mass production. This review summarizes the recent studies on gas sensors based on hematite nanostructures. It also provides useful insights into various strategies for enhancing the gas-sensing properties of gas sensors based on hematite nanostructures.

Keywords : Gas sensor, Hematite, Nanostructure, Oxide semiconductor.

1. INTRODUCTION

Gas sensors based on semiconducting metal oxides have garnered extensive interest in varied applications such as medical diagnosis, environmental monitoring, artificial olfactory, and mobile applications, owing to their small-scale, cost-effective, and simple operation [1,2]. To date, diverse oxide materials including SnO_2, TiO_2, WO_3, and ZnO have been researched for gas sensor applications. Among them, hematite (α-Fe_2O_3) is considered a promising gas-sensing material because of its chemical stability and appropriate bandgap energy (2.2 eV). Furthermore, hematite is the most prolific and cheapest metal oxide semiconductor obtained from the earth crust. As reported by the U.S. Geological Institute, the world iron resources were estimated to be 800 billion tons, and the amount of annual world iron production was described as up to 3.1 billion tons in 2012 (Fig. 1) [3]. This amount is approximately four-thousand times higher than that of Sn, whose oxide form (SnO_2) is currently the most widely used metal oxide semiconductor in gas sensors. Although large amounts of iron have been mined and refined annually over the past nine years (2012–2021), its reserves have remained virtually unchanged, whereas tin reserves have declined by 12%, from 5 million tons to 4.2 million tons. Despite the potential strength in economic aspects and sustainability of hematite, its potential should be first investigated thoroughly in gas sensor applications owing to its inferior sensitivities, slow response, and low selectivity compared with gas sensors based on SnO_2 [4,5].

Considering their large surface-to-volume ratio, enhanced surface activity, and high adsorption/desorption ratio toward target gas molecules, nanostructures designed from metal oxides are considered one of the prospective ways to improve gas-sensing performance [6,7]. Accordingly, various hematite nanostructures, right from zero-dimensional (0-D) nanoparticles to three-dimensional (3-D) hierarchy structures, synthesized using various procedures such as hydrothermal, anodic oxidization, and e-beam evaporation, have been explored for use in gas sensors [8-15]. As a result, the gas-sensing performance (sensitivity, response time, and selectivity) of hematite-based gas sensors have been enhanced dramatically; however, several issues still remain in field applications, including poor long-term stability and variation in sample fabrication procedures.

This paper summarizes the various approaches used for synthesizing gas sensors based on various hematite nanostructures,

[1] Department of Materials Science and Engineering, Research Institute of Advanced Materials, Seoul National University Gwanak-ro 1, Gwanak-gu, Seoul 08826, Republic of Korea
[2] Advanced Institute of Convergence Technology, Seoul National University, Suwon 16229, Republic of Korea
[+] Corresponding author: hwjang@snu.ac.kr
(Received: Jul. 7, 2021, Revised: Jul. 20, 2021, Accepted: Jul. 23, 2021)

This is an Open Access article distributed under the terms of the Creative Commons Attribution Non-Commercial License(https://creativecommons.org/licenses/by-nc/3.0/) which permits unrestricted non-commercial use, distribution, and reproduction in any medium, provided the original work is properly cited.

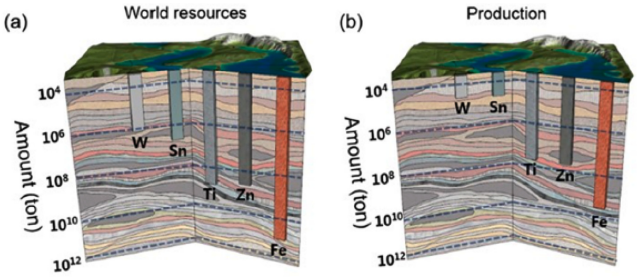

Fig. 1. Total mineral resources on earth and production in 2012 for W, Sn, Ti, Zn, and Fe as per U.S. Geological Survey. Reprinted with permission from [9]. Copyright © 2015, American Chemical Society.

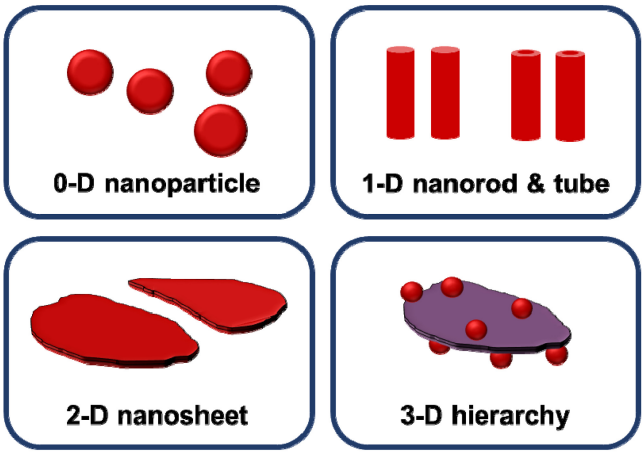

Fig. 2. Schematics of various nanostructures, from 0-D to 3-D.

such as 0-D nanoparticles, 1-D nanotubes, 2-D nanosheets, and 3-D hierarchical structures, including the procedures and gas-sensing properties of each strategy. Furthermore, we introduce a 3-D hierarchical structure incorporated with hetero-species of metal oxides and compare its gas-sensing characteristics with those of various hematite nanostructure-based gas sensors. This review is expected to provide valuable insight into the development of highly cost-effective hematite nanostructure-based gas sensors.

2. HEMATITE NANOSTRUCTURE-BASED GAS SENSORS

Various nanostructures classified according to their dimensions are presented in Fig. 2. Nanostructures with a high surface-area-to-volume ratio can be formed into various shapes depending on the synthesis method and experimental conditions. Using this characteristic, we can improve the disadvantages of hematite-based gas sensors, namely, low reactivity and slow reaction rate.

2.1 0-D nanoparticles

The simplest nanostructure, a 0-D nanoparticle, is the most widely used nanostructure for hematite gas sensors, and sensors based on 0-D nanomaterials have the advantage of abundant active sites and high surface-to-volume ratios. Hjiri et al. reported a NO_2-selective sensor based on hematite nanoparticles synthesized via the hydrothermal method. For the synthesis, a solution was prepared by mixing $FeCl_3$ (0.1 M) with ammonia (2 mL) and heated at 200 °C for 10 h in a steel autoclave. The resultant material was washed several times and dried at 60 °C for 1 h. In the final step, the obtained powder was annealed for 2 h at 500 °C. The synthesized powder was then analyzed using the X-ray diffraction technique (XRD). The diffraction peaks in Fig. 3(a) show only hematite peaks, indicating that the annealing had completely changed β-FeOOH to the hematite phase. Fig. 3(b) shows the scanning electron microscopy (SEM) images of the hematite nanoparticles. As revealed in several researches [13,16,17], hematite powders prepared via the hydrothermal method are 1.5–2.5 μm in diameter owing to the agglomeration of smaller nanoparticles. Fig. 3(c) shows the transmission electron microscopy (TEM) image of the hematite nanoparticles, which shows hexagonal nanoparticles with an average crystalline size of approximately 50 nm. The high-resolution transmission electron microscopy (HRTEM) image in Fig. 3(d) indicates the high crystallinity of the grains. The fabricated hematite nanoparticles were placed on an alumina substrate to measure their gas-sensing performance. To optimize the operational temperature, response measurements to 5 ppm NO_2 were obtained for temperatures from 150 °C to 300 °C, as shown in Fig. 3(e). The hematite nanoparticles showed the best response (3.4) at 200 °C. For evaluating the selectivity, the authors exposed the specimen to three different gases: NO_2, CO, and CO_2. The bar chart in Fig. 3(f) shows the response values to the target gases, in addition to those toward NH_3 and methane. The response to NO_2 was higher than that to other gases because of the high affinity of NO_2 for hematite [18]. Fig. 3(g) displays the dynamic response values of hematite nanoparticles to NO_2 (in 1–5 ppm concentrations). In the measured concentration range, the hematite nanoparticles showed linear sensitivity. The response and recovery times of the hematite nanoparticles are presented in Fig. 3(h). The response time reduced from 72 s to 10 s with an increase in the target gas concentration from 1 ppm to 5 ppm. However, the recovery time increased from 8 s to 180 s in the same concentration range owing to gas adsorption kinetics [18]. This work clearly demonstrated that

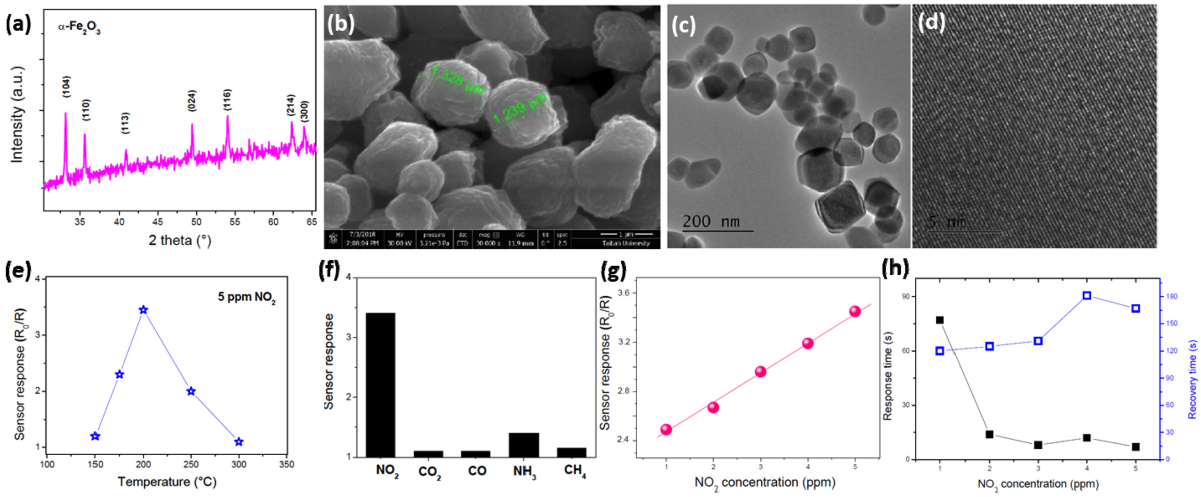

Fig. 3. (a) XRD pattern, (b) SEM image, (c) TEM image, (d) HRTEM image of the hematite nanoparticles, (e) Response values for 5 ppm NO_2, (f) Response values to NO_2, CO_2, CO, NH_3, and CH_4 at 200 °C, (g) Response values to NO_2 for 1–5 ppm concentrations at 200 °C, (h) Response and recovery time values of the hematite nanoparticles. Reprinted with permission from [8]. Copyright © 2019, MDPI.

the gas-sensing performance of hematite nanoparticles synthesized via the hydrothermal method ensures NO_2 selectivity.

2.2 1-D nanotubes

1-D nanostructures include nanorods, nanowires, nanofibers, and nanotubes. Various methods such as thermal oxidation, e-beam evaporation, chemical vapor deposition, and anodic oxidation are used to synthesize these nanostructures [9,19–22]. Compared to 0-D nanostructures, 1-D nanostructures show better transduction of the surface phenomenon into the electrical resistance change of the sensor. Kim et al. reported a vertically ordered hematite nanotube array using the anodic oxidation method. An Fe film was deposited on a patterned Pt electrode-SiO_2/Si substrate of 500 nm thickness using an electron beam evaporator. After the deposition, anodization was conducted in an ethylene glycol solution containing ammonium fluoride and water with a Pt cathode and Fe film anode, as shown in Fig. 4(a). Anodization for 3 min resulted in films composed of 1.2 μm hematite nanotubes. Finally, the amorphous hematite nanotube layer was annealed at 550 °C for 5 h and turned into a 1 μm-thick crystalline hematite film. Fig. 4(b) shows the SEM images of the hematite nanotube array. The cross-sectional image confirms that the Fe film was completely converted into a hematite nanotube array. Moreover, the XRD patterns display no metallic Fe peak for the as-anodized nanotube array, as visible in Fig. 4(d). Furthermore, the hematite nanotube array after annealing shows sharp hematite phase peaks without secondary phases. The TEM images in Fig. 4(c) clearly show that the vertically ordered nanotube array has uniform diameters. The selected-area electron diffraction (SAED) pattern shows the polycrystalline characteristics of the nanotube array after annealing. After the fabrication procedure, the dense, planar hematite film and hematite nanotube array were exposed to 50 ppm acetone at 350 °C. Both specimens responded rapidly to acetone with a decrease in resistance. However, the hematite nanotube array showed an approximately 10 times higher response compared to the dense, planar hematite film (Fig. 4(e)). To test the selectivity of the hematite nanotube arrays to acetone, responses to various target gases were measured, including ethanol, CO, H_2, C_6H_6, C_7H_8, NH_3, and CH_4. Evidently, the hematite nanotube array showed the highest sensitivity to acetone (84) [23,24]. The response ratio of acetone to the second most sensitive gas, ethanol, i.e., $S_{acetone}/S_{ethanol}$, was higher than 2.1. The responses of the dense-planar hematite film to these target gases were also measured, and the results are plotted in Fig. 4(f). Compared to reference dense, planar hematite films, the hematite nanotube array showed higher sensitivity and selectivity toward acetone gas. In addition to good sensitivity, the hematite nanotube array also exhibited a short response time of approximately 3 s in 90% responses, as shown in Fig. 4(g), which is much shorter than that demonstrated by the dense-planar hematite film (28 s). From Fig. 4(h), the responses of the hematite nanotube array to 1–5 ppm concentrations of acetone are 10.28, 13.21, 15.6, 17.7, and 20.1, respectively. From these response values, the theoretical detection limit for acetone is calculated to be approximately 1.71 ppb. Furthermore, according to Fig. 4(i), the response values for

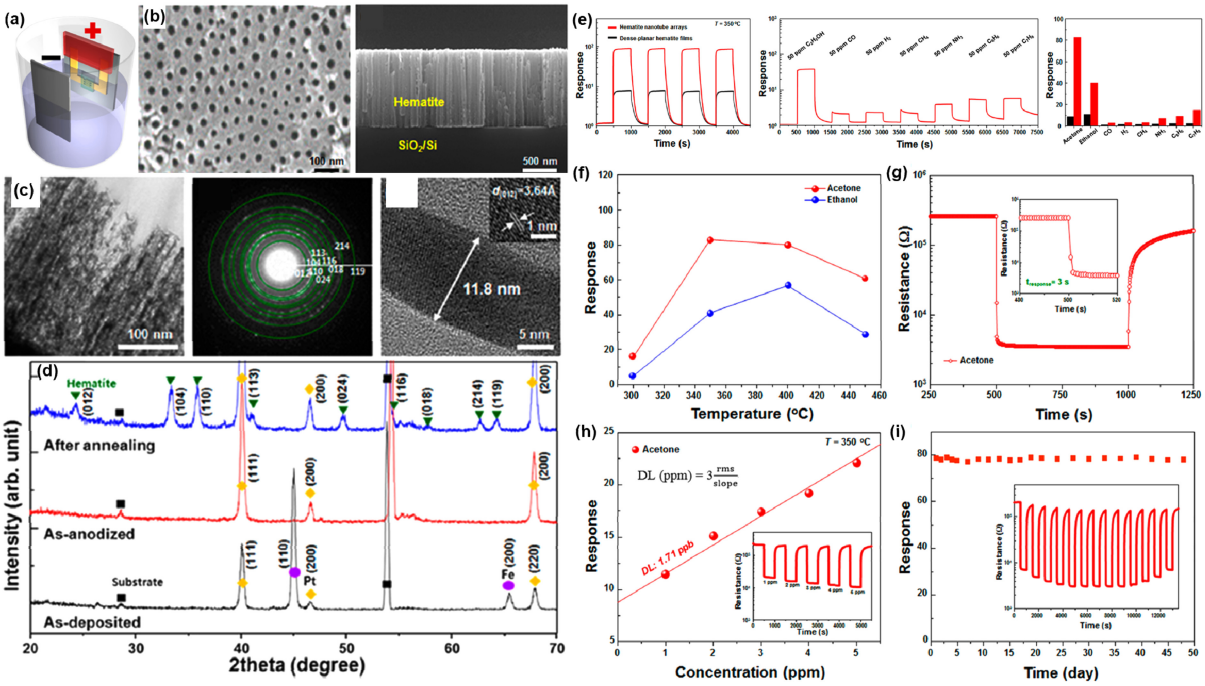

Fig. 4. (a) Schematic showing the anodizing method to create a hematite nanotube array on Pt interdigitated electrode (IDE)-patterned SiO_2/Si substrate, (b) Plain-view and cross-sectional SEM images of a hematite nanotube array, (c) Cross-sectional TEM images, SAED pattern with indexing, HRTEM image of the wall thickness of a hematite nanotube, (d) Glancing angle XRD patterns of an Fe/Pt/SiO_2/Si structure before anodization and hematite nanotube arrays before and after annealing at 550 °C for 5 h, (e) Dynamic sensing transient curve of a dense, planar hematite film and hematite nanotube array; sensing transients to various gases for the hematite nanotube array; and response values of the dense, planar hematite film and hematite nanotube array to various gases at 350 °C, (f) Responses of the hematite nanotube array to 50 ppm acetone and ethanol, (g) Dynamic acetone sensing transient of hematite nanotube array at 350 °C. Inset: 90% response time ($t_{response}$) of the hematite nanotube array, (h) Theoretical detection limit (DL) of hematite nanotube array to acetone. Inset: response curve of the hematite nanotube array to 1−5 ppm acetone at 350 °C, (i) Changes in the response of hematite nanotube array to 50 ppm acetone for 48 days. Inset: response to 13 consecutive pulses of 10−50 ppm acetone after 48 days. Reprinted with permission from [9]. Copyright © 2014, American Chemical Society.

hematite nanorods indicate long-term stability, with sustained response values for 48 days. These results suggest that the introduction of 1-D nanotube structures promises extremely high sensitivity, great selectivity, and long-term stability to hematite-based gas sensors.

2.3 2-D nanoporous films

2-D nanostructures represented by graphene have a high aspect ratio; therefore, they have numerous surface sites to react with gaseous molecules. Ma et al. reported the gas-sensing properties and mechanism of network structures assembled from hematite nanosheets with exposed {104} facets. This work was based on previously reported research, which stated that hematite nanostructures with specific exposed facets, such as {012}, {01$\bar{4}$}, and {$\bar{2}$10} exhibited enhanced gas-sensing performance toward CH_3COCH_3 and C_2H_5OH [25]. In this work, the hematite network structures were synthesized by heating $Fe(NO_3)_3$ solution containing PVP at 650 °C in air. Fig. 5(a) shows SEM images of the products prepared using the synthesizing process. The network structures assembled from hematite nanosheets have a thickness of approximately 23–34 nm. The XRD diffraction peaks are indexed as hexagonal structures of hematite. The TEM images confirm that the hematite nanosheet is single crystalline and enclosed by {104} facets. To optimize the operating temperature, gas sensors based on the hematite nanosheet network structures were exposed to 100 ppm C_2H_5OH and $N(C_2H_5)_3$ at different temperatures. The maximum measured response was at 300 °C. The gas-sensing performance of the sensors based on the hematite nanosheet network structure was compared with that of sensors based on hematite commercial powders. After being exposed to various concentrations of C_2H_5OH and $N(C_2H_5)_3$, both sensors exhibited a short response time and good reversibility, as shown in Fig. 5(b). However, the response value curve of the two types of sensors to C_2H_5OH and $N(C_2H_5)_3$ revealed that the hematite nanosheet network structures display a higher response than hematite nanopowders to all measured concentrations. To explain

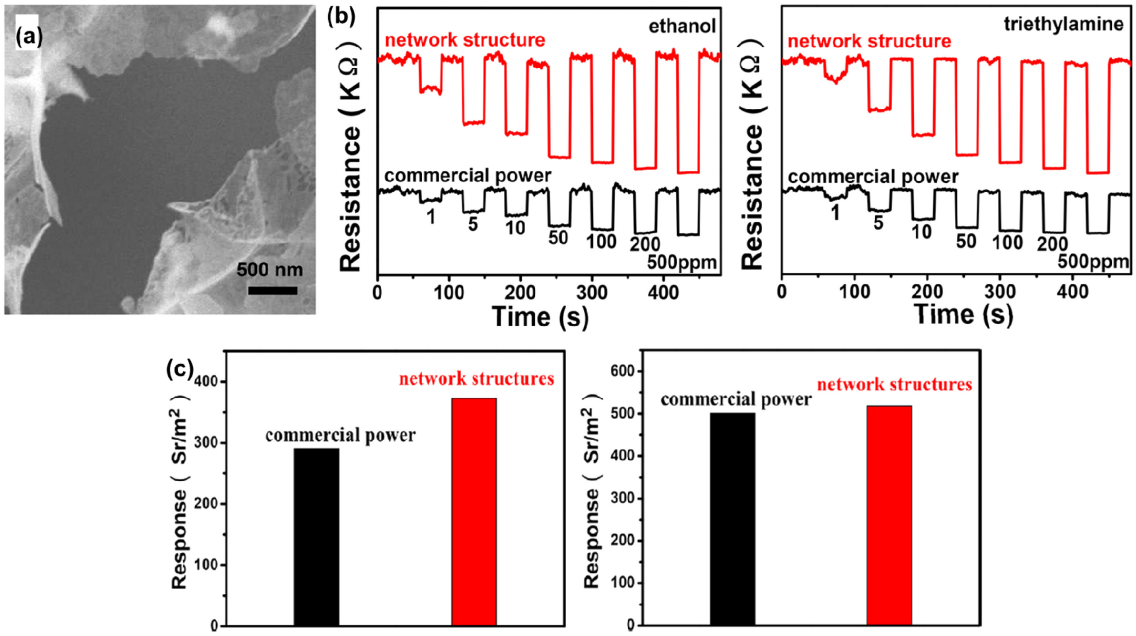

Fig. 5. (a) SEM images of hematite nanosheet network structure, (b) Response and recovery curve of the hematite nanosheet network structure and hematite commercial powder sensor, (c) Responses (per unit surface area) of hematite nanosheet network structure and hematite commercial powder sensor to 100 ppm C_2H_5OH and $N(C_2H_5)_3$. Reprinted with permission from [10]. Copyright © 2017, American Chemical Society.

the difference in the sensing properties, the sample's response per unit surface area to 100 ppm of C_2H_5OH and $N(C_2H_5)_3$ was calculated and plotted, as shown in Fig. 5(c). The normalized response value of the hematite nanosheet network structure is evidently higher than that of hematite commercial powder, implying that hematite nanosheets with exposed {104} facets exhibit much better gas-sensing performance than hematite commercial powders. Furthermore, the XPS spectra of hematite nanosheet network structures and commercial powders revealed oxygen adsorption ability. The hematite nanosheet network structures had more chemisorbed oxygen species and O_2-ions in oxygen-deficient regions than hematite commercial powders, indicating a superior oxygen chemisorbing ability and a higher number of oxygen vacancies. These results suggest that controlling the exposed facets of hematite nanosheets results in extraordinary gas-sensing performance.

2.4 3-D hierarchical heterostructure

3-D nanostructures exhibit the most complex and diverse morphology. Because of the possibility of heterojunctions, 3-D hierarchical heterostructures are being actively studied [26]. The different Fermi levels of two metal oxide semiconductors comprising heterostructures generates a potential barrier at their interfaces, which is an essential factor in enhancing the gas-sensing properties of sensors based on heterojunctions [27]. Suh et al. reported a selective toluene sensor based on hematite-decorated nickel oxide nanocorals. Fig. 6(a) shows a schematic of the preparation method for hematite-decorated nickel oxide nanocorals. Vertically ordered nickel oxide nanorods with hematite decoration were deposited on an SiO_2/Si substrate with Pt-interdigitated electrodes using the glancing angle deposition method based on electron beam evaporation. A 100 nm thick nickel oxide nanorod layer was deposited with a tilt angle of 83°, followed by a 3 nm-thick Fe layer deposition at a tilt angle of 0°. The deposition procedure was repeated until the total thickness reached approximately 600 nm. The nickel oxide and iron films were annealed at 550 °C for 2 h to oxidize iron into hematite. The SEM images in Fig. 6(b) show the typically smooth and extremely rough surfaces of the bare nickel oxide nanorods and hematite-decorated nickel oxide nanocorals, respectively. The repetitive Fe layer deposition between NiO nanorods caused an adhesion force change between the Fe layers and NiO, yielding a rough surface [28]. Energy dispersive X-ray spectroscopy (EDS) mapping (Fig. 6(c)) of hematite-decorated nickel oxide nanocorals revealed a uniform distribution of Ni and O elements and sparse distribution of the Fe element, which indicates that the Fe film was converted to nanoparticles. The authors manipulated the deposition angle of

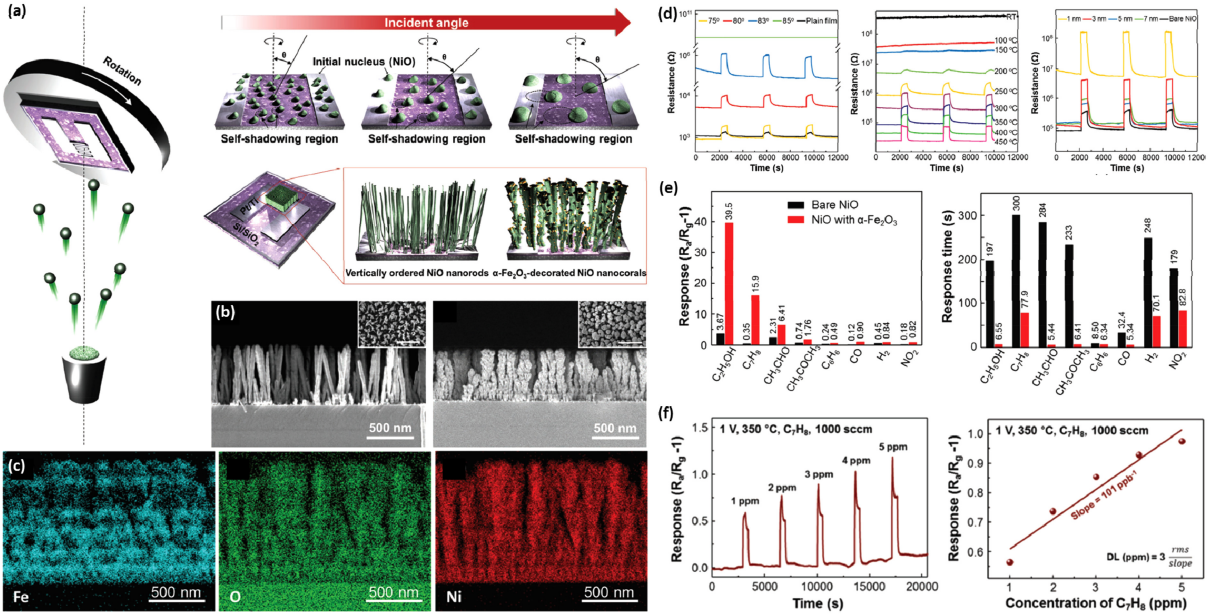

Fig. 6. (a) Schematic of glancing angle deposition, self-shadowing effects when increasing the incident angle, and vertically ordered NiO nanorods without and with hematite decoration, (b) Cross-sectional SEM images of NiO nanorods without and with hematite decoration, (c) EDS mapping of Fe, O, and Ni for hematite-decorated NiO nanocorals. (d) Response transient curves of bare NiO nanorods according to incident angles, operating temperature, and Fe interlayer thickness, (e) Response and response-time values for bare NiO nanorods and hematite-decorated NiO nanocorals to various gases (5 ppm for NO_2 and 50 ppm for other gases), (f) Responses and calibration of response for hematite-decorated NiO nanocorals to 1–5 ppm C_7H_8 at 350 °C. Reprinted with permission from [11]. Copyright © 2017 WILEY-VCH Verlag GmbH & Co. KGaA.

nickel oxide nanorods (75°, 80°, 83°, and 85°) to control their density (Fig. 6(d)). After being exposed to 50 ppm C_2H_5OH, the nickel oxide nanorods deposited on the substrate at a tilt angle of 83° exhibited the maximum response. For optimizing the gas-sensing performance further, the operating temperature and thickness of Fe film deposition were modified. The optimal conditions for ensuring a high sensing performance from hematite-decorated nickel oxide nanocorals were determined to be an operational temperature of 350 °C and Fe-film deposition thickness of 3 nm. Furthermore, the VOC selectivity at optimum conditions was measured from the responses of bare nickel oxide nanorods and hematite-decorated nickel oxide nanocorals to various gases, including C_2H_5OH, C_7H_8, CH_3CHO, CH_3COCH_3, C_6H_6, CO, NO_2, and H_2. As shown in Fig. 6(e), both specimens displayed the highest response to C_2H_5OH. However, there was a difference in the second highest response, with bare nickel oxide nanorods responding to CH_3CHO and hematite-decorated nickel oxide nanocorals to C_7H_8. Especially, the response ratio of hematite-decorated nickel oxide nanocorals to bare nickel oxide nanorods for C_7H_8 showed an extremely high value, which is sufficient to allow selective detection of C_7H_8. To study the selectivity more deeply, the authors investigated the detection results for three consecutive pulses of various gases based on Principal Component Analysis (PCA). Bare nickel oxide nanorods did not show any obvious selectivity because of the overlapping area of most gases. However, hematite-decorated nickel oxide nanocorals showed excellent selectivity and a clear distinction to various gases, especially C_7H_8. To investigate the possibility of practical application, the long-term stability and humidity dependence were also investigated. The response curve to eight consecutive pulses of 50 ppm C_7H_8 for 30000 s confirmed their stability. Humidity induced a sharp increase in the base resistance; however, the gas response of hematite-decorated nickel oxide nanocorals to C_7H_8 was maintained. The response values of hematite-decorated nickel oxide nanocorals were observed as 0.38, 0.48, 0.53, 0.55, and 0.59 to 1–5 ppm C_7H_8, respectively, at 350 °C, as shown in Fig. 6(f). From these response values, the slope of the concentration–response curve was calculated to be 101 ppb^{-1}, and the theoretical detection limit was calculated to be 22 ppb. Therefore, a suitably designed metal oxide heterostructure and fully decorated nanostructure can be effective for developing gas sensors. The comparative gas-sensing properties of gas sensors based on various hematite nanostructures are listed in Table 1.

Table 1. Gas-sensing performances of gas sensors based on hematite nanostructures.

Nanostructures	Gas concentration	Sensitivity ($\Delta R/R_0$)	Response time (s)	Recovery time (s)	Operating temperature (°C)	Reference
0-D nanoparticle	5 ppm NO_2	3.4	8	180	200	8
0-D hollow particle	50 ppm C_2H_5OH	1.77	4	15	400	13
0-D hollow nanoparticle	100 ppm C_2H_5OH	15	6	21	300	12
1-D nanotube	50 ppm CH_3COCH_3	84	3	-	350	9
2-D nanosheet network structure	100 ppm C_2H_5OH	6	-	-	300	10
3-D hierarchy NiO/hematite	50 ppm C_2H_5OH	39.5	6.55	-	350	11

3. CONCLUSION

In this article, we reviewed the use of hematite nanostructures in gas sensors. Various methods have been introduced to enhance the performance of gas sensors using the properties of nanostructures, such as large surface-to-volume ratio, enhanced surface activity, and high adsorption/desorption ratio of target gas molecules. In particular, the low reactivity and slow response time, which are the disadvantages of hematite-based gas sensors, were improved. Based on these results, we intend to pave the way for hematite-based gas sensors to play an active role as a key sensing material in various high-performance gas-sensing fields. With this strategy, we hope that hematite, the most abundant and cheapest material in the earth's crust, will become a key material for next-generation gas-sensing technologies.

ACKNOWLEDGMENT

This research was supported by the Strategic Core Material Development Program through the Korea Evaluation Institute of Industrial Technology (KEIT) funded by the Ministry of Trade, Industry and Energy (MOTIE) (No.10080736). The Inter-University Semiconductor Research Center and Institute of Engineering Research at Seoul National University provided research facilities for this work.

REFERENCES

[1] N. Yamazoe and K. Shimanoe, "Proposal of contact potential promoted oxide semiconductor gas sensor", *Sens. Actuator B-Chem.*, Vol. 187, pp. 162–167, 2013.

[2] I. S. Hwang, Y. S. Kim, S. J. Kim, B. K. Ju, and J. H. Lee, "A facile fabrication of semiconductor nanowires gas sensor using PDMS patterning and solution deposition", *Sens. Actuator B-Chem.*, Vol. 136, No. 1, pp. 224–229, 2009.

[3] http://www.usgs.gov/ (retrieved on Jul. 23, 2021).

[4] L. Liao, Z. Zheng, B. Yan, J. X. Zhang, H. Gong, J. C. Li, C. Liu, Z. X. Shen, and T. Yu, "Morphology controllable synthesis of α-Fe_2O_3 1D nanostructures: Growth mechanism and nanodevice based on single nanowire", *J. Phys. Chem. C*, Vol. 112, No. 29, pp. 10784–10788, 2008.

[5] Z. Wu, K. Yu, S. Zhang, and Y. Xie, "Hematite hollow spheres with a mesoporous shell: Controlled synthesis and applications in gas sensor and lithium ion batteries", *J. Phys. Chem. C*, Vol. 112, No. 30, pp. 11307–11313, 2008.

[6] X. Pan, X. Liu, A. Bermak, and Z. Fan, "Self-gating effect induced large performance improvement of ZnO nanocomb gas sensors", *ACS Nano*, Vol. 7, No. 10, pp. 9318–9324, 2013.

[7] S. Shao, X. Qiu, D. He, R. Koehn, N. Guan, X. Lu, N. Bao, and C. A. Grimes, "Low temperature crystallization of transparent, highly ordered nanoporous SnO_2 thin films: Application to room-temperature hydrogen sensing", *Nanoscale*, Vol. 3, No. 10, pp. 4283–4289, 2011.

[8] M. Hjiri, M. S. Aida, and G. Neri, "NO_2 selective sensor based on α- Fe_2O_3 nanoparticles synthesized via hydrothermal technique", *Sensors (Switzerland)*, Vol. 19, No. 1, p. 167, 2019.

[9] D. H. Kim, Y. S. Shim, J. M. Jeon, H. Y. Jeong, S. S. Park, Y. W. Kim, J. S. Kim, J. H. Lee, and H. W. Jang, "Vertically ordered hematite nanotube array as an ultrasensitive and rapid response acetone sensor", *ACS Appl. Mater. Interfaces*, Vol. 6, No. 17, pp. 14779–14784, 2014.

[10] Y. Ma, J. Yang, Y. Yuan, H. Zhao, Q. Shi, F. Zhang, C. Pei, B. Liu, and H. Yang, "Enhanced Gas Sensitivity and Sensing Mechanism of Network Structures Assembled from α-Fe_2O_3 Nanosheets with Exposed {104} Facets," *Langmuir*, Vol. 33, No. 35, pp. 8671–8678, 2017.

[11] J. M. Suh, Y. S. Shim, D. H. Kim, W. Sohn, Y. Jung, S. Y. Lee, S. Choi, Y. H. Kim, J. M. Jeon, K. Hong, K. C. Kwon, S. Y. Park, C. Kim, J. H. Lee, C. Y. Kang, and H. W. Jang., "Synergetically Selective Toluene Sensing in Hematite-Decorated Nickel Oxide Nanocorals", *Adv. Mater. Technol.*, Vol. 2, No. 3, p. 1600259, 2017.

[12] C. Jin, C. Ge, G. Xu, G. Peterson, Z. Jian, Y. Wei, and K. Zhu, "Influence of nanoparticle size on ethanol gas sensing performance of mesoporous α-Fe_2O_3 hollow spheres", *Mater Sci Eng B*, Vol. 224, pp. 158–162, 2017.

[13] C. M. Hung, N. D. Hoa, N. Van Duy, N. Van Toan, D. T. T. Le, and N. Van Hieu, "Synthesis and gas-sensing char-

acteristics of α- Fe_2O_3 hollow balls", *J Sci-Adv Mater Dev*, Vol. 1, No. 1, pp. 45–50, 2016.

[14] J. Huang, M. Yang, C. Gu, M. Zhai, Y. Sun, and J. Liu, "Hematite solid and hollow spindles: Selective synthesis and application in gas sensor and photocatalysis", *Mater. Res. Bull.*, Vol. 46, No. 8, pp. 1211–1218, 2011.

[15] Z. Cao, Z. Jiang, L. Cao, Y. Wang, C. Feng, C. Huang, and Y. Li, "Lattice expansion and oxygen vacancy of α- Fe_2O_3 during gas sensing", *Talanta*, Vol. 221, p. 121616, 2021.

[16] W. X. Jin, S. Y. Ma, Z. Z. Tie, X. H. Jiang, W. Q. Li, J. Luo, X. L. Xu, and T. T. Wang, "Hydrothermal synthesis of monodisperse porous cube, cake and spheroid-like α- Fe_2O_3 particles and their high gas-sensing properties", *Sens. Actuator B-Chem.*, Vol. 220, pp. 243–254, 2015.

[17] Q. Z. Zeng, S. Y. Ma, W. X. Jin, H. M. Yang, H. Chen, Q. Ge, and L. Ma, "Hydrothermal synthesis of monodisperse α- Fe_2O_3 hollow microspheroids and their high gas-sensing properties", *J. Alloys Compd.*, Vol. 705, pp. 427–437, 2017.

[18] S. T. Navale, D. K. Bandgar, S. R. Nalage, G. D. Khuspe, M. A. Chougule, Y. D. Kolekar, Shashwati Sen, and V. B. Patil, "Synthesis of Fe_2O_3 nanoparticles for nitrogen dioxide gas sensing applications", *Ceram. Int.*, Vol. 39, No. 6, pp. 6453–6460, 2013.

[19] L. Yuan, Q. Jiang, J. Wang, and G. Zhou, "The growth of hematite nanobelts and nanowires-tune the shape via oxygen gas pressure", *J. Mater. Res. Technol.*, Vol. 27, pp. 1014–1021, 2012.

[20] Y. S. Shim, K. C. Kwon, J. M. Suh, K. S. Choi, Y. G. Song, W. Sohn, S. Choi, K. Hong, J. M. Jeon, S. P. Hong, S. Kim, S. Y. Kim, C. Y. Kang, and H. W. Jang, "Synthesis of Numerous Edge Sites in MoS_2 via SiO_2 Nanorods Platform for Highly Sensitive Gas Sensor", *ACS Appl. Mater. Interfaces*, Vol. 10, No. 37, pp. 31594–31602, 2018.

[21] D. H. Kim, T. H. Kim, W. Sohn, J. M. Suh, Y. S. Shim, K. C. Kwon, K. Hong, S. Choi, H. G. Byun, J. H. Lee, and H. W. Jang,, "Au decoration of vertical hematite nanotube arrays for further selective detection of acetone in exhaled breath", *Sens. Actuator B-Chem.*, Vol. 274, pp. 587–594, 2018.

[22] Y. G. Song, Y. S. Shim, J. M. Suh, M. S. Noh, G. S. Kim, K. S. Choi, B. Jeong, S. Kim, H. W. Jang, B. K. Ju, and C. Y. Kang, "Ionic-Activated Chemiresistive Gas Sensors for Room-Temperature Operation", *Small*, Vol. 15, No. 40, p. 1902065, 2019.

[23] Y. Xia, H. Dai, H. Jiang, L. Zhang, J. Deng, and Y. Liu, "Three-dimensionally ordered and wormhole-like mesoporous iron oxide catalysts highly active for the oxidation of acetone and methanol", *J. Hazard. Mater.*, Vol. 186, No. 1, pp. 84–91, 2011.

[24] G. Picasso, A. Quintilla, M. P. Pina, and J. Herguido, "Total combustion of methyl-ethyl ketone over Fe_2O_3 based catalytic membrane reactors", *Appl. Catal. B*, Vol. 46, No. 1, pp. 133–143, 2003.

[25] X. Li, W. Wei, S. Wang, L. Kuai, and B. Geng, "Single-crystalline α-Fe_2O_3 oblique nanoparallelepipeds: High-yield synthesis, growth mechanism and structure enhanced gas-sensing properties", *Nanoscale*, Vol. 3, No. 2, pp. 718–724, 2011.

[26] K. C. Kwon, J. M. Suh, T. H. Lee, K. S. Choi, K. Hong, Y. G. Song, Y. S. Shim, M. Shokouhimehr, C.-Y. Kang, S. Y. Kim, and H. W. Jang, "SnS_2 Nanograins on Porous SiO_2 Nanorods Template for Highly Sensitive NO_2 Sensor at Room Temperature with Excellent Recovery", *ACS Sensors*, Vol. 4, No. 3, pp. 678–686, 2019.

[27] S. Yang, G. Lei, H. Xu, Z. Lan, Z. Wang, and H. Gu, "Metal oxide based heterojunctions for gas sensors: A review", *Nanomaterials*, Vol. 11, No. 4, pp. 1–26, 2021.

[28] K. Marre and H. Neddermeyer, "Growth of ordered thin films of NiO on Ag(100) and Au(111)", *Surf. Sci.*, Vol. 287, pp. 995–999, 1993.